ORIGINAL ARTICLE

Multiclass Supervised Learning Approach for SAR-COV2 Severity and Scope Prediction: SC2SSP Framework

Shaik Khasim Saheb [1*], B. Narayanan [2], T. V. Narayana Rao [3]

[1] *Department of Computer Science and Engineering, Sreenidhi Institute of Science and Technology, Hyderabad, India*

[2] *Faculty of Engineering & Technology, Annamalai University, Chidambaram, India*

[3] *Professor of CSE and HoD-CSE IOT in Sreenidhi Institute of Science and Technology, Hyderabad, India*

*Corresponding Author: Shaik Khasim Saheb
Email: khasim.s@sreenidhi.edu.in

Received: 21 February 2023 / Accepted: 22 July 2023

Abstract

Purpose: Identifying high-risk areas for the virus or the potential for the technique to be applied to this infectious disease might be difficult. The existing tools being used for predicting viruses exhibit various limitations. The severe pneumonia caused by the rapidly spreading coronavirus disease (COVID-19) is predicted to have a significant negative impact on the healthcare sector. Accurate treatment requires an urgent need for early diagnosis, which reduces pressure on the healthcare system. Computed Tomography (CT) scan and Chest X-Ray (CXR) are some of the standard image diagnoses. Although a CT scan is the most common method for diagnosis, CXR is the most frequently utilized since it is more accessible, quicker, and less expensive.

Materials and Methods: In this manuscript, the proposed model SC2SSP is a multiclass supervised learning technique that aims to predict the scope and severity of the SAR-COV2 virus using data on confirmed cases and deaths. The model may also utilize preprocessing techniques which are Gaussian smoothing for handling imbalanced data, such as oversampling or under sampling, as well as feature extraction methods such as Local Binary Pattern to identify the most relevant input features for the prediction task. Additionally, a classifier such as XGBoost can also be used to further improve the model's performance. This makes the model more robust and accurate in predicting the scope and severity of the SAR-COV2 virus.

Results: The model utilizes the Exact Greedy Algorithm to classify the spread and impact of the virus in different regions. The performance metrics like accuracy, precision, fscore and sensitivity are analyzing the proposed method performance. The proposed SC2SSP approach attains 3.101% and 7.12% higher accuracy; 24.13% and 13.04% higher precision compared with existing methods, like the Detection of COVID-19 from Chest X-ray Images Using Convolutional Neural Networks (Resnet50), Deep learning for automated recognition of covid-19 from chest X-ray images (VGGNet), respectively.

Conclusion: The conclusion and potential future healthcare planning follow the exploration of evidence-based approaches and modalities in the scope and forecast.

Keywords: Supervised Learning; COVID-19; Deep Learning; Neural Nets.

DOI:

Frontiers in BIOMEDICAL TECHNOLOGIES

1. Introduction

There have been many epidemics that have affected humans in the past. To defeat these pandemics, the WHO (World Health Organization) is cooperating with some national authorities and clinicians. The first case of COVID-19 disease has been confirmed in Wuhan, china Dec 2019, it spread globally. On January 30, 2020, this epidemic was declared an international concern by the WHO [1, 2]. Coronavirus Disease 2019 (COVID-19) is the official name of a respiratory infectious disease caused by a new coronavirus that started first in Wuhan. Severe acute respiratory syndrome coronavirus-2 (SARS-CoV-2) is a novel type of virus, which has not been recognized in people earlier [3-5]. The virus primarily spreads through respiratory problems, droplets from coughing and sneezing, or when people come into contact with each other [6]. People become infected with this virus if their hands come in contact with their nose, eyes, or mouth when these droplets are inhaled or they may land on surfaces that other people may touch.

Because this virus can remain for days in the environment and on food-contact surfaces like plastic, wood, rubber, and stainless steel, meat tissue surfaces may be a viable or possibly crucial channel for COVID-19 infection transmission. Nevertheless, the amount of possible viruses may fall off after some time and would not always exist to cause infection [7]. Vaccination campaigns have been critical in combating the spread of COVID-19. By September 2021, multiple vaccines were authorized for emergency use, and many countries had initiated vaccination programs. However, predicting the exact outcome of these vaccination efforts is challenging due to various factors, including vaccine availability, distribution challenges, vaccine hesitancy, and the emergence of new variants. It's important to continue monitoring the efficacy of existing vaccines against new variants and the need for potential booster shots. COVID-19 vaccines are by no means a silver bullet. With more COVID-19 vaccines awaiting approval in the coming months, it is important to note that vaccine availability does not equate to vaccine access or vaccine efficacy. According to some studies, the COVID-19 vaccination won't be available to 9 out of 10 people living in low-income nations until 2023 or later. If vaccinated individuals are few, the proposed method full effort to sort out this issue and predict the result for a large number accurately. Additionally, in cases involving people, symptoms of the virus can be seen between 1 and 14 days after the first infection. Later, it began to spread quickly, leaving no time for defense against a newly discovered, notorious, and contagious virus, which compelled the WHO to declare COVID-19 to be more pandemic due to rapid transmission among people [8]. Numerous individuals have already contracted the disease, and many lives have also been lost. The clinical department has been conducting a number of trials to evaluate the efficacy of COVID-19, but no findings have been made public to date. Since it is a novel virus, there is also no vaccine available. Although many pharmaceutical and research firms have begun to work on the vaccine, it may take months or perhaps a year before the vaccine is accessible to humans [9]. Because of an inadequate number of ventilators, hospital beds, kits, and oxygen tanks and no proper treatment available or no vaccine availability, it is prominent to examine the positive cases increment, amount of recovery cases, and other aspects, which might impact the virus growth. Everyone should be aware of this virus and take the appropriate actions to overcome it. The main contributions are summarized as follows,

- This paper proposes an efficient SC2SSP method to comprehensively integrate the contextual clues of infected regions that aims to predict the scope and severity of the SAR-COV2 virus using data on confirmed cases and deaths. The proposed SC2SSP model utilizes an exact greedy algorithm to classify the spread and impact of the virus in different regions. For handling imbalanced data, a Gaussian smoothing filter is used.

- Benefiting from more elaborate existing methods, the proposed SC2SSP framework can better profile the most essential pathological manifestation from the simplest samples to complex ones in a self-paced way. As a result, the current small-sample dataset's performance is assured. Feature extraction methods such as Local Binary Pattern are to identify the most relevant input features for the prediction task. Moreover, classifier such as XGBoost is used to improve the model's performance.

- A well-established SAR-COV2 dataset with multilevel annotations is constructed to fill the data gap for automated SAR-COV2 and facilitate related research. Experimental outcomes on the SAR-COV2 data set demonstrate the superiorities of our SC2SSP framework

for automatic SAR-COV2 in comparison with state-of-the-art baselines.

The remaining part of this manuscript is arranged as follows: the related work is described in Segment 2, the materials and methods are demonstrated in Segment 3, the experimental section is described in Segment 4, and the conclusion section is described in Segment 5.

1.1. Related Works

Accurate outbreak assessment methods should be used to provide insight and spread the cause of the disease. The legislative scheme includes enforcement and oversight measures but remains a co-regulation model rather than a direct regulation model. The work [11] presents the contemporary worldwide pandemic illness COVID-19 has been intended intricate and non-linear nature. Moreover, the epidemics have variances with other contemporary epidemics that raise a query to recognize the standard mode's ability to provide exact results [12]. Some known and unknown variables involved in the spread, the difficulty of wide population activities in geo-political domains, and variances in containment schemes had increased method uncertainty deeply [13]. Accordingly, the standard epidemiological methods face novel challenges for delivering more consistent outcomes. To overcome this challenge, numerous novel methods have evolved that introduce various assumptions toward modeling [14-16]. Machine learning enhances the screening procedure and diagnosis of recognized patients through radio imaging schemes similar to blood sample data and Computed Tomography (CT). Healthcare expert utilizes radiology imageries, like CT scans and X-rays as routine devices for enhancing conventional screening and diagnosis. At the peak of the SARS-CoV-2 pandemic outbreak, such devices' performance is only modest, which is inappropriate. The work [17] expresses feasible ML devices by suggesting a new approach for the rapid SARS-CoV2 diagnosis model.

An ancillary device was presented under deep learning to enhance the accuracy [18]. The 127 infected patients' raw chest X-ray pictures were used in the model. The binary class accuracy of 98.08% and the multiclass accuracy of 87.02% have both been obtained with excellent performance. The multi-class envisioned the use of expert systems to aid radiology in quickly and properly confirming the screening process. By integrating laboratory, clinical, and demographic data with percentages of CD3, GHS, total protein, and patient age while using SVM as a major feature classification approach, multiple studies have discovered four key medical features. [19]. The simulation results showed that the integration of 4 characteristics results in an AUROC of 0.9757 and 0.9996 in the testing and training datasets in respective order, demonstrating that the novel method was reliable and effective in estimating patients in severe or critical circumstances.

Wherein, 253 clinical blood samples from Wuhan were examined, and 11 significant associated indices that could serve as a discrimination tool for COVID-19 over healthcare professionals who are skilled in rapid diagnosis were found by various studies [20]. The contributions demonstrated that 11 associated indices were retrieved using the Random Forest (RF) algorithm, with the specificity of 96.97% and an accuracy of 95.95%. Applications of AI and ML have been utilized to forecast and estimate the current pandemic status. The AI and ML applications have been used in predicting and estimating the existing pandemic situation. The innovative method, which utilized stacking-ensemble through an SVM regression algorithm on cumulative positive COVID-19 instances from Brazilian data, assessed and projected the outcomes of 10 patients overall in each of the 10 states of Brazil within 1-6 days. As a result, the short-term prediction process is improved, alerting healthcare professionals and the government to prepare for pandemics [21]. A novel approach utilizing a supervised recursive multi-layered classifier known as XGBoost was presented on mammographic and clinical parameter datasets. Following the method's implementation, the researchers discovered three standout characteristics from 75 clinical characteristics and blood test results samples that had 90% accuracy in calculating and classifying COVID-19 patients as general, moderate, and severe [22].

The forecast approach engaged decision rule for forecasting quickly and estimates the infected people at maximal risk, the patients who declared as infected must be deemed for intensive care. The Canadian-based time-series forecasting method has been

created using a deep-learning algorithm over a large short-term memory network. According to the research [23], multiple researchers have discovered a crucial parameter that is intended for assessing the course and predicting the end of the current SARS-CoV-2 outbreak in Canada as well as throughout the universe. The SARS-CoV-2 pandemic was expected to terminate in Canada around June 2020, according to the suggested method. According to data collected from the University of John Hopkins, according to the work [24], the estimation is probably accurate because the number of new infected cases has decreased quickly. The time series technique based on autoregressive integrated moving average and the goodness of forecasting model based on wavelet have been combined to project the realistic forecasting method [25].

Prediction of the COVID-19 scope from the target patient's clinical records was the goal of contemporary contributions. The severity (mortality scope) of the diseased patient prediction was critical to treat the patient with a personalized course of medical recommendations; even if computer-assisted clinical practices were undoubtedly necessary to increase the sensitivity and specificity of the COVID-19 prognosis. This publication provided a statistical analysis scale with regard to the goal of mortality scope prediction.

Gradient Boosting Survival Model (GBSM) [26] explored the presentation of diversified supervised learning approaches to forecasting the mortality scope of the diseased individuals, who were tested positive in COVID-19 test. The Individual-Level Fatality Prediction Model [27], which was inspired by Gradient Boosting Survival Model's discharge time prediction [26], has worked to determine the range of artificial intelligence techniques for predicting the individual fatality scope of patients who have tested positive for the covid-19. However, their contributions were based on demographic data, which may or may not contain any chronic diseases. In these recent contributions, the additional demographic characteristics associated with health conditions have not been considered. The suggested method has utilized a variety of factors linked to clinical diagnosis outcomes of the patients to forecast the severity of the COVID-19 infection in a person who tested positive for the infection after receiving a COVID-19 test.

2. Materials and Methods

Chest X-rays, abbreviated CXR radiographs, of patients classified as high, medium, low, and healthy were used as critical input to the proposed model. The class label "high" indicates a high risk of mortality, "medium" indicates the need for ICU services often with mechanical ventilation, "low" indicates the need for home isolation with close monitoring of oxygen saturations, and "healthy" indicates a negative test result. Preprocessing the input radiographs to produce higher-quality source radiographs with less noise can be accomplished using any of the well-known image processing noise filters. The resulting image in this case contains residual effects from background subtraction. As a result, the preprocessing phase also includes segmentation of the source radiographs in order to differentiate the Region Of Interest (ROI) from the surrounding areas of the source images. The final image would be a waveform with the least possible effect on the boundary. Additionally, the CXR ROI border with a thick border is smoothed during the preprocessing phase.

2.1. Computation of Gradients

Within the features of HOG, a localized 1-D histogram of edge directions is accumulated across the pixels of each of the cells by splitting the picture window into tiny spatial sections called cells. The gradient values are computed throughout the calculation. Applying the 1-D centered, the mask of point-discrete derivatives at either of the horizontal as well as vertical axes is the most typical approach. This approach necessitates filtering the image's color or intensity data using the filtering kernels [1,0, -1] as well as [1, 0, -1]. The filter "Gaussian-smoothing" was used to produce the gradients, which were then tested using one of many masks of discrete derivatives.

2.2. Binning by Orientation

The next stage in the HOG features is to calculate the cell histograms. Depending on the direction of the

gradient component placed on it, each of the pixels calculates Histogram Channel's weighted-vote, and then, the votes are aggregated into orientation-bins across small spatial areas called cells. Cells might be radial or rectangular in shape. According to the gradient's sign, which is either "signed" or "unsigned", the bins are uniformly spaced between "0-degree and "180-degree or 360-degree". The matching bin has been found for the orientation of each of the pixels.

2.3. Block of Descriptors

The gradient intensities in the Features extra4ted must be localized. The cells must be normalized, which means they must be grouped together into bigger, physically related blocks. The HOG description is the fusion of the elements and portions of each block region's cell histograms that are in normal form. These blocks frequently overlap, implying that each of these cells contributes to the final description more than once. There are two types of block geometries: the blocks of R-HOG that are in a rectangle shape and the blocks of C-HOG that are in a circle shape.

2.4. Normalization Block

Block normalization may be done in four distinct ways. Let V be the quasi vector representing histograms of a particular block, where ||VI|K is its k-norm for 1<=k<=e a tiny constant of approximate value. The normalizing value is then chosen from the list below (Equation 1):

$$L_2norm = \boldsymbol{v} * \sqrt{(||\boldsymbol{v}||_2 + \boldsymbol{e}^2) - 1} \quad (1)$$

L2-hys: As in, L2-norm, clipping (v<= 0.2), and converts it again to normal form as follows and is defined in Equations 2 and 3,

$$L_1norm = v * (|v||_1 + e)^{-1} \quad (2)$$

$$L_1sqrt = \sqrt{v * (||v||_2 + e) - 1} \quad (3)$$

Furthermore, the L2-hys technique may be determined by considering the L2-norm, the clipped result, and performing normalizing again.

2.5. Features of LBP

LBP (Local-Binary Pattern) is the description of an image, which explores how that image appears in a limited area surrounding a pixel. The fundamental LBP-operator was based on the premise that texture delivers two distinct items locally: a pattern and the intensity of that pattern. The LBP-operator operates on a 3X3 block of pixels of the given image. To produce a tag for the central pixel, the block's pixels should be thresholded by the intensity of the central pixel, multiplied by squares, and then aggregated. The neighborhood consists of 8 pixels, hence there are a total of 28 = 256 labels that may be made using the appropriate grey-values of the neighborhood's other pixels and its center pixel [13]. Along with global features, the average and deviation of LBP-region level features of an image are determined and utilized in classification. We use the following notation for the LBP operator: LBP_{PR}^{u2}. The subscript represents using the operator in a PR neighborhood. Superscript $u2$ stands for using only uniform patterns and labeling all remaining patterns with a single label. A histogram of the labeled data $f1(x, y)$ can be defined in Equation 4,

$$H_i = \sum_{x,y} I\{f1(x, y) = i, i = 0,1, \ldots . n - 1\} \quad (4)$$

Here n represents the number of different labels created by the LBP operator and is defined in Equation 5:

$$I(A) = \begin{cases} 0A \; is \; true \\ 1A \; is \; false \end{cases} \quad (5)$$

This histogram contains information about the distribution of the local micro patterns. For efficient representation, one should retain spatial information. For this intention, the data is separated as regions, and the enhanced histogram is defined in Equation 6:

$$H_{i,j} = \sum_{x,y} I\{f1(x, y) = i\} \quad (6)$$

$$I(x, y) \in R_j, i = 0 \ldots n - 1, j = 0 \ldots m - 1$$

2.6. The Features

To train the classifiers, CXRs were evaluated. In this case, the given CXR images will be processed to extract the region of interest, which is the infected lung's white mass. Feature engineering is applied to detect suggested features in a CXR radiograph. To train the chosen classifier, diverse characteristics listed as "Haralick texture features", "HOG (Histogram of Oriented Gradients) features", and "LBP (Local Binary Pattern) features" should be engineered further.

2.7. Haralick Texture Features

The texture of a picture may be measured using the co-occurrence matrix, which is dependent on the image's gray-scale values or intensity, as well as multiple color dimensions. Because these matrices (of co-occurrence) are large and dispersed, several measures of the two-dimensional matrix are investigated for a specific set of characteristics. The two matrices are turned at different angles (0 degree, 45 degrees, 90 degrees, as well as 135 degrees) and various characteristics are assessed; these features are known as Haralick texture features and are retrieved from the enlarged picture. The Grey-Level Co-occurrence Matrix (GLCM) of dimension Ng, wherein Ng represents multiple intensity levels in the given radiograph, is a square matrix. The matrix element indexed at (i, j) is created by counting how many instances a pixel with index 'i' is next to a pixel at index 'J'. Further divides the complete matrix with the count of comparisons done. Each item represents the likelihood of a pixel with index 'i' being next to a pixel with index 'J'.

2.8. HOG Features

The HOG (Histogram of Oriented-Gradients) is a global image descriptor that is mostly used for object recognition in IP (image processing) as well as CV (computer vision). A number of times gradient orientation occurs in some areas of the picture [12]. Regional object aspect and form inside an image are described by the dispersion of intensity-gradients or edge-information, which is a key notion underpinning the histogram of directed gradients descriptor. The input image is segmented as small linked sections denoted as cells, and HOG is developed for the pixels of each cell. The conjunction of the stated histograms is used as the descriptor. Regional histograms can indeed be normalized for better accuracy by computing an approximation of the intensity throughout a wider region of the picture, known as a block, and then each of the cells within a block will be normalized by using the resultant value. Because of this normalization, the inversion of changes in light and shading is improved [28-30].

In this histogram, three different levels of the locality are illustrated: Information about the patterns is contained in the histogram's labels, which are summarized across a limited area to produce information at the regional level, and the regional histograms are concatenated to create a global description. When the data is divided into regions, it is anticipated that some regions have valuable information than others in terms of distinguishing betwixt people. To benefit from this, a weight can be assigned for each region according to the significance of the data it contains. For example, the weighted χ^2 statistic is specified in Equation 7:

$$\chi^2(extractedfeatures) = \sum_{i,j} w_j\,(extractedfeatures)^2 \qquad (7)$$

Let w_j as a weight for region$j$. Table 1 shows the set of extracted features.

2.9. Feature Optimization

The task of Feature optimization discovers the HOG features, Haralick texture features, and local binary patterns that are exclusive or more optimal towards the radiograph images of exclusive class labels. The MWU-Test (Mann-Whitney U Test) [31] does not involve a centric distribution format that is required in most datasets with diverse labels. Since this test is a non-parametric test, it makes no assumptions about score distribution. However, various assumptions are made, such as the randomness of the observation selected from the population, the independence of the observations and bilateral independence, and the use of an arbitrary measuring tool. This non-parametric test is an alternative to an independent t-test. It's used to see if two samples are from the same population or if the given observations are larger than the other

observations. The MWU-Test implementation process is described beneath.

The notations v_1 and v_2 denote vector distributions taken as input to the MWU-Test to determine the scope of diversity betwixt corresponding vectors. Initially, all the entries of vectors $v_1$and v_2 are moved to a new vector. The vector v is sorted in ascending order values and considers the indices of the ordered values of the vector v as corresponding ranks R. The rank of each identical value is determined by the

Table 1. The List of Haralick Features

Entropy of difference	The difference between an image's entropy values
Correlation information measures 1 and 2	The expression of the variables' combined probability density distributions decreases the conventional correlation coefficient.
Correlation coefficient with the greatest value.	The interaction of pixels in a radiograph on a linear scale
Contrast.	The difference between the maximum and least pixel values is measured.
Second angular moment (ASM).	The metric gauges the homogeneity of a picture.
Variance.	The average of squared deviations from the image's mean
Total variance	The sum of the image's variance values
Entropy.	The quantity of data that should be used for a radiograph
Average of the sum	The aggregate of all the image's mean values
Variance in comparison	The difference between an image's variance values
Correlation	The Grey levels of adjacent pixels in the picture have a linear relationship.
Total entropy	The entire quantity of data that must be encoded in a picture

average of its indices. The ranks allocate to vector values v_1 as set R_1 and the ranks allocate to vector values v_2 as set R_2. Then the process finds the aggregate of the entries in the set R, as RS_1, which determines the rank-sum threshold RST of the vector, and is exhibited in Equation 8,

$$RST1 = RS1 = \frac{1v1x(Iv11+1)}{2} \quad (8)$$

In the notation lv, I denotes the size of the vector v_1.

Similarly, the rank-sum threshold RST of the vector v_2 will be determined as follows and is defined in Equation 9:

$$RST_1 = RS2 = \frac{1v2x(Iv21+1)}{2} \quad (9)$$

In notational v_2, I implies the size of vector v_2, the notation RS implies a sum of entries rank in vector v_2 that is listed in set R_2.

The rank-sum threshold RST of vector entries v_1, v_2 is the sum of rank-sum thresholds RST, RST_2 of the vectors v_1, v_2 followed and is defined in Equation 10:

$$RST1 = RS1 + RST2 \quad (10)$$

Determine the z-score [32] as below:

Initially, the mean Mrst and standard deviation Drst is defined by Equations 11 and 12:

$$mRST = \frac{RST}{2} \quad (11)$$

$$dRST = \sqrt{\frac{|V1\,|*v|+1)|}{|v|}} = \sqrt{\frac{|V1\,|*|v2|)|}{|v|}}\lceil |v|+1\rceil - \sum_{il}^{k}\frac{t3-t1}{|v|*(|v|-1)}\rceil \ldots \quad (12)$$

The notation k signifies the number of separate rankings, and the notation t stands for a number of elements with the same rank.

The z-core is expressed in Equation 13,

$$Z = \frac{RST - m_{RST}}{d_{RST}} \quad (13)$$

Then find the p-value of depicted z score in z-table [33]. The vectors v_1, v_2 are assumed as diverse if the p-value is higher than the provided probability threshold (typically 0.1, 0.05, or 0.01). Otherwise, the

distribution of vectors is similar. Finally, extracted features are fed to the classification technique.

2.10. Classification Approach

XGBoost is a widely used and fast implementation of the Gradient-Boosted Trees-based classification technique [34], which is built on expression optimization via the approximation of certain loss-expressions as well as the use of multiple regularization strategies. At an iteration t, the objective-expression which is the conjunction of loss-expression plus regularization strategies) that intends to minimize is as follows: The XGBoost objective of fitness is recurrent expressions, which is of recurrent CART learners that cannot be maximized using typical Euclid space optimization approaches [35]. As an illustration, it can be stated that the optimum linear estimate for f(x) at position 'a' is [36] (Figure 1):

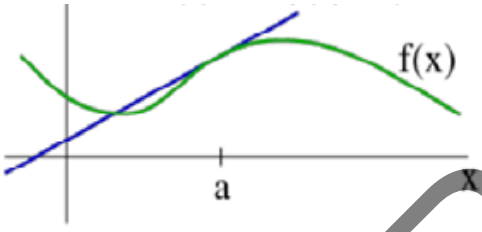

Figure 1. f(a) + f'(a)(x-a)

It is necessary to apply the Taylor approximations so we must convert the initial fitness expression to the Euclidean space in order to employ conventional optimization methods.

Consider the simplest linear approximate solutions of the expression f(x) as follows and is defined in Equation 14:

$$f(x) \approx f(a)f'(a)(x-a)$$
$$\Delta X = f_t(x_i) \quad (14)$$

The initial expression is merely Ax. Using Taylor's principle, we can convert f(x) to a minimal expression of x around a point 'a'. Before the Taylor approximation, the fitness expression f(x) was the summation of t CART trees, but now it is merely the step t (present tree). Discrete fitness expression is required. The predicted value (t-1) is ax, the new learner that needs to be added at step t, and f(x) is the loss expression 1 this time. This allows us to use different methods to optimize the Euclidean space by defining the loss expression as a simple expression of each independent learner newly added. As previously indicated, the estimate at the previous step (t-1) is 'a,' and the new learner (x-a) that required at step t. As a result of using the second-order Taylor approximation, we obtain:

$f(t) \approx f(a)(x-a) + \frac{1}{2}f^x(a)(x-a)2$	XG Boost Objective Using Second-order Taylor approximation
$£^{(t)} \approx \sum_{t-1}^{n}(t(y_{11}\, y^{(t-1)} - g_1 f_t(x_i) + \frac{1}{2}h_i f_1^2(x_i)] + \Omega(f_t)$	
Where:	
$g = \partial_g(x - 1)t(y_{t1}\, y^{(t-1)} and\ h_i = \partial_g^2(t-1)(y_{11}y^{(t-1)})$	The loss expression's Ist as well as 2nd ordered gradient stats

The loss expression's 1st and 2nd ordered gradient statistics finally; removing the constant components yields the following concise reduction aim at active step t:

$£^{(t)} = \sum_{t-1}^{n}(g_{1f_1}(x_1) + \frac{1}{2}h_{1f_t^2}(x_1)\| + \Omega(f_t)$	XGBoost basic objective

The next objective is to achieve a learner that maximizes the loss-expression at present iteration t, because the former is a summation of the quadratic units of a single variable that can be reduced using well-known techniques.

$argmin_z Gx + \frac{1}{2}Hx^2 = -\frac{G}{H}, H > 0\ min_z\ Gx + \frac{1}{2}Hx^2 = -\frac{1}{2}\frac{G2}{H}$	Reduce a basic quadratic formula to its simplest form

Iteration t requires the development of a learner that achieves the highest potential loss reduction. Hence, there is a method for "assessing the efficacy of a tree structure q," and the scoring expression with accurate prediction is as follows and is defined in Equation 15:

$$£^{(t)}(q) = -\frac{1}{2}\sum_{j=1}^{T} k\frac{(\sum_{iCij} gi)2}{\sum_{i€ij,} h_{i+\lambda}} + \gamma T \qquad (15)$$

It is extremely difficult to "enumerate all potential tree architectures k=1 throughout the program and q" and hence locate the tree with the greatest control of the loss.

Notably, the aforementioned "quality scoring expression with accurate prediction" returns the smallest loss assigned to a given tree structure, meaning that the actual loss expression is evaluated using appropriate weights. Therefore this model has achieved higher accuracy in predicting the scope and severity of the SAR-COV2 virus. For computing the optimal leaf weights, every tree topology is considered.

In action, the following is performed to grow the learner:

Begin with a single root (take all of the training samples)

Recurrent over all characteristics and their associated values, evaluating each conceivable decrease in splitting loss:

Gain = ($loss_{ib}$ – $loss_{rb}$) – ($loss_{ib}$ – $loss_{rb}$)	Loss of left branch $loss_{ib}$,loss of right branch $loss_{rb}$

The positive gain shall be expected from the optimal splitting, which should be greater than the min splitting gain argument, else the branch will cease developing. The algorithm described above is referred to as the "Exact Greedy Algorithm" with O(n*m) complexity, wherein n denotes the count of training instances and m denotes the dimensionality of the characteristics.

Consider the following scenario of two-class classification as well as the logging loss expression:

$yIn(p) + (1-y)In(1-p) where\ p = \frac{1}{(1+e^{-z})}$	Two – class classification having Cross – Entropy loss expression,

Wherein y is the actual label in the range 0 to 1 as well as p denotes the approximated probability. Notably, p (estimate or quasi-probability) has to be derived after the exponential expression is applied to the result of the GBT prototype x. The model's output x is the aggregate of the learners of the CART-tree.

Thus, to reduce the log-loss optimization approach, it must first determine its first and second derivative (gradient as well as hessian) in regard to x. You may get gradient = (p-y) as well as hessian = p* at thread (1-p). Learners will aim to limit the log loss goal, as well as the leaf level scores, which are actual weights that reflect the significance as a sum across all available trees in the model are always altered to reduce the loss, by synthesizing the GBT approach, which is an aggregate of CART scores. As a consequence, the sigmoid activation expression should be applied to the output of GBT modeling techniques in the form of a two-class classification likelihood score. From the sigmoid expression, the exact greedy algorithm can clearly classify the spread and impact of the virus in different regions.

3. Results

3.1. The Data

The input X-rays with labels (Positive or negative) have been adopted from the renowned dataset called BIMCV-COVID19+ [37]. The chest X-rays are intended to cover a wide spectrum of thoracic entities, which is a significant escalation of the dataset set quality compare to the majority of existing datasets [28-30]. The other significance of the dataset is the high resolution of the chest X-ray images. The first version of the dataset contains 1380 chest X-rays. Performance is analyzed under the mentioned performance metrics [38-40]. The obtained results are assessed with existing approaches, such as COVID-19 diagnosis from Chest X-Ray Images Using Convolutional Neural Networks RES-NET50 [10] and Deep learning for automated identification

of COVID-19 from chest X-ray images VGGNet [17].

3.1.1. Performance Measures

This is a significant task for classifier selection. To examine the performance, performance metrics are examined. To scale the performance metrics, the following confusion matrix is needed.

- TP: It is an actual count of positives properly predicted by a model over total positives.
- TN: It is an actual count of negatives properly predicted by a model over the total negatives.
- FP: It is the result of a number of negatives wrongly predicted, divided by the total negatives.
- FN: It is the result of a number of positives wrongly predicted, divided by the total positives.

3.1.2. Accuracy

It is defined as the whole number of proceedings at the dataset and is represented in Equation 16,

$$Accuracy = \frac{(TP + TN)}{(TP + TN + FP + FN)} \quad (16)$$

3.1.3. Precision

This is the classifier capability to calculate the extracted features without any conditions and is represented in Equation 17,

$$Precision = \frac{TP}{(TP + FP)} \quad (17)$$

3.1.4. Recall

It is a computation of the amount of real positives that is correctly foreseeable and is represented in Equation 18,

$$Sensitivity = \frac{TP}{FN + FP} \quad (18)$$

3.1.5. F-score

It is computed using Equation 19,

$$F - score = \frac{2TP}{(2TP + FP + FN)} \quad (19)$$

3.1.6. Performance Analysis

Table 2-5 shows an analysis of the proposed SC2SSP method. The performance metrics like precision, sensitivity, fscore, and accuracy is analyzed. Here the proposed SC2SSP technique is compared to the existing methods such as Resnet50 and VGGNet, respectively.

Table 2 demonstrates the Comparison for precision. Here, the proposed SC2SSP method provides 32.21%, 37.56% higher precision for fold 1 at class high; 25.45%, 45.89% higher precision for fold 1 at class moderate; 56.34%, 21.23% higher precision for fold 1 at class low; 25.45%, 45.89% higher precision for fold 1 at class normal; 21.1%, 32.2% higher precision for fold 2 at class high; 34.4%, 32.2% higher precision for fold 2 at class moderate; 33.5%, 22.2% higher precision for fold 2 at class low; 33.6%, 33.4% higher precision for fold 2 at class normal; 56.6%, 54.4% higher precision for fold 3 at class high; 22.2%, 55.4% higher precision for fold 3 at class moderate; 23.3%, 56.6% higher precision for fold 3 at class low; 22.1%, 54.4% higher precision for fold 3 at class normal; 55.3%, 33.2% higher precision for fold 4 at class high; 22.1%, 33.4% higher precision for fold 4 at class moderate: 33.6%, 55.4% higher precision for fold 4 at class low; 44.3%, 32.2% higher precision for fold

Table 2. Comparison for precision

Methods	Precision															
	Fold 1				Fold 2				Fold 3				Fold 4			
	H	M	L	N	H	M	L	N	H	M	L	N	H	M	L	N
Resnet50	0.2	0.4	0.6	0.8	0.45	0.3	0.3	0.11	0.75	0.66	0.7	0.4	0.1	0.5	0.8	0.6
VGGNet	0.3	0.5	0.2	0.1	0.46	0.6	0.1	0.7	0.8	0.7	0.6	0.2	0.8	0.3	0.9	0.8
SC2SSP (proposed)	1	1	1	1	1	1	1	1	1	1	1	1	1	1	1	1

H: High; M: Medium; N: Normal; L: Low

4 at class normal evaluated to the existing methods Resnet50 and VGGNet, respectively.

Table 3 demonstrates the Comparison for sensitivity. Here, the proposed SC2SSP method provides 30.21%, 38.56% higher sensitivity for fold 1 at class high; 25.45%, 45.89% higher sensitivity for fold 1 at class moderate; 56.34%, 21.23% higher sensitivity for fold 1 at class low; 25.45%, 45.89% higher sensitivity for fold 1 at class normal; 21.1%, 32.2% higher sensitivity for fold 2 at class high; 34.4%, 32.2% higher sensitivity for fold 2 at class moderate; 33.5%, 22.2% higher sensitivity for fold 2 at class low; 33.6%, 33.4% higher sensitivity for fold 2 at class normal; 56.6%, 54.4% higher sensitivity for fold 3 at class high; 22.2%, 55.4% higher sensitivity for fold 3 at class moderate; 23.3%, 56.6% higher sensitivity for fold 3 at class low; 22.1%, 54.4% higher sensitivity for fold 3 at class normal; 55.3%, 33.2% higher sensitivity for fold 4 at class high; 22.1%, 33.4% higher sensitivity for fold 4 at class moderate: 33.6%, 55.4% higher sensitivity for fold 4 at class low; 44.3%, 32.2% higher sensitivity for fold 4 at class normal evaluated to the existing methods Resnet50 and VGGNet, respectively.

Table 4 demonstrates the Comparison for fscore. Here, the proposed SC2SSP method provides 30.21%, 38.56% higher fscore for fold 1 at class high; 25.45%, 45.89% higher fscore for fold 1 at class moderate; 56.34%, 21.23% higher fscore for fold 1 at class low; 25.45%, 45.89% higher fscore for fold 1 at class normal; 21.1%, 32.2% higher fscore for fold 2 at class high; 34.4%, 32.2% higher fscore for fold 2 at class moderate; 33.5%, 22.2% higher fscore for fold 2 at class low; 33.6%, 33.4% higher fscore for fold 2 at class normal; 56.6%, 54.4% higher fscore for fold 3 at class high; 22.2%, 55.4% higher fscore for fold 3 at class moderate; 23.3%, 56.6% higher fscore for fold 3 at class low; 22.1%, 54.4% higher fscore for fold 3 at class normal; 55.3%, 33.2% higher fscore for fold 4 at class high; 22.1%, 33.4% higher fscore for fold 4 at class moderate: 33.6%, 55.4% higher fscore for fold 4 at class low; 44.3%, 32.2% higher fscore for fold 4 at class normal evaluated to the existing methods Resnet50 and VGGNet, respectively.

Table 5 demonstrates the Comparison for accuracy. Since a lack of accurate and timely predictions of the spread and impact of the virus, the proposed method helps to address one of the critical challenges in the fight against the pandemic. The approach used in this study leverages machine learning algorithms to analyze large amounts of data, allowing for more comprehensive and accurate predictions. The results of this study have significant implications for public health decision-making, as they can inform the development of more effective intervention strategies and the allocation of resources. This study also highlights the importance of interdisciplinary collaborations between researchers in computer science, mathematics, and public health. The integration of different perspectives and expertise is crucial in addressing complex global health challenges like the SAR-COV2 pandemic. Existing automated SAR-COV2 generally faces single-measurement and small-sample learning issues. To deal with these issues, a novel SC2SSP framework is proposed which can successfully use multi-view learning and self-paced learning mechanisms for quantitative analysis of SAR-COV2. When analyzed to the existing methods, the proposed SC2SSP comprehensively aggregates the multi-view contextual clues of lung infections that predict the scope and severity of the SAR-COV2 virus using data on confirmed cases and deaths. With

Table 3. Comparison for sensitivity

Methods	Sensitivity															
	Fold 1				Fold 2				Fold 3				Fold 4			
	H	M	L	N	H	M	L	N	H	M	L	N	H	M	L	N
Resnet50	0.2	0.41	0.63	0.81	0.45	0.36	0.32	0.11	0.75	0.66	0.75	0.45	0.19	0.50	0.85	0.65
VGGNet	0.3	0.52	0.25	0.18	0.46	0.65	0.45	0.75	0.83	0.73	0.68	0.26	0.85	0.39	0.76	0.83
SC2SSP (proposed)	0.92	0.9	0.93	0.9	0.91	0.95	0.91	0.94	0.96	0.92	0.96	0.92	0.93	0.9	0.9	0.91

H: High; M: Medium; N: Normal; L: Low

Table 4. Comparison for fscore

Methods	Fscore															
	Fold 1				Fold 2				Fold 3				Fold 4			
	H	M	L	N	H	M	L	N	H	M	L	N	H	M	L	N
Resnet50	0.2	0.41	0.63	0.81	0.45	0.36	0.32	0.11	0.75	0.66	0.75	0.45	0.19	0.50	0.85	0.65
VGGNet	0.3	0.52	0.25	0.18	0.46	0.65	0.45	0.75	0.83	0.73	0.68	0.26	0.85	0.39	0.76	0.83
SC2SSP (proposed)	0.92	0.9	0.93	0.9	0.91	0.95	0.91	0.94	0.96	0.92	0.96	0.92	0.93	0.9	0.9	0.91

H: High; M: Medium; N: Normal; L: Low

Table 5. Comparison for Accuracy

Methods	Accuracy															
	Fold 1				Fold 2				Fold 3				Fold 4			
	H	M	L	N	H	M	L	N	H	M	L	N	H	M	L	N
Resnet50	0.23	0.43	0.66	0.83	0.47	0.35	0.39	0.18	0.75	0.61	0.78	0.47	0.20	0.57	0.87	0.65
VGGNet	0.35	0.58	0.26	0.19	0.48	0.68	0.44	0.77	0.83	0.76	0.68	0.28	0.85	0.39	0.76	0.83
SC2SSP (proposed)	0.92	0.91	0.91	0.9	0.91	0.95	0.91	0.98	0.96	0.92	0.96	0.92	0.93	0.9	0.9	0.91

H: High; M: Medium; N: Normal; L: Low

a self-paced learning method to help the SC2SSP learn from simple to complicated, the combined algorithm is introduced to categorize the spread and impact of the virus in various regions and ensure the performance of SC2SSP under the current small sample condition. The experimental results on the SAR-COV2 dataset prove the potential of the proposed SC2SSP framework. Here, the proposed SC2SSP method provides 30.21%, 38.56% higher accuracy for fold 1 at class high; 25.45%, 45.89% higher accuracy for fold 1 at class moderate; 56.34%, 21.23% higher accuracy for fold 1 at class low; 25.45%, 45.89% higher accuracy for fold 1 at class normal; 21.1%, 32.2% higher accuracy for fold 2 at class high; 34.4%, 32.2% higher accuracy for fold 2 at class moderate; 33.5%, 22.2% higher accuracy for fold 2 at class low; 33.6%, 33.4% higher accuracy for fold 2 at class normal; 56.6%, 54.4% higher accuracy for fold 3 at class high; 22.2%, 55.4% higher accuracy for fold 3 at class moderate; 23.3%, 56.6% higher accuracy for fold 3 at class low; 22.1%, 54.4% higher accuracy for fold 3 at class normal; 55.3%, 33.2% higher accuracy for fold 4 at class high; 22.1%, 33.4% higher accuracy for fold 4 at class moderate: 33.6%, 55.4% higher accuracy for fold 4 at class low; 44.3%, 32.2% higher accuracy for fold 4 at class normal evaluated to the existing methods Resnet50 and VGGNet, respectively.

3.2. Clinical Evaluation

Clinical evaluation involves the assessment of patients based on their signs, symptoms, and medical history. It aims to diagnose and monitor the progression of COVID-19. Here are some components of clinical evaluation:

a) Medical History: Gathering information about the patient's symptoms, exposure history, and any underlying medical conditions that may increase the risk or severity of COVID-19.

b) Physical Examination: Assessing the patient's vital signs (temperature, heart rate, respiratory rate), lung sounds, and any specific signs indicative of COVID-19, such as cough, shortness of breath, or loss of taste and smell.

c) Laboratory Tests: Conducting various laboratory tests to aid in COVID-19 diagnosis and monitor disease progression. These tests include molecular tests (e.g., PCR) to detect the presence of the SARS-CoV-2 virus, serological tests to detect antibodies against the virus, and blood tests to assess organ function and inflammatory markers.

d) Radiological Imaging: Using imaging techniques like chest X-rays or Computed Tomography (CT) scans to evaluate lung involvement and identify

any characteristic findings associated with COVID-19, such as ground-glass opacities.

e) Severity Assessment: Evaluating the severity of COVID-19 based on established criteria, which may include the patient's clinical presentation, oxygen saturation levels, and need for hospitalization or intensive care.

3.3. Qualitative Evaluation

Qualitative evaluation focuses on understanding the lived experiences, perspectives, and perceptions of individuals affected by COVID-19. It involves qualitative research methods to gather subjective data. Here are some approaches used in qualitative evaluation:

a) Interviews: Conducting individual or group interviews with COVID-19 patients, healthcare workers, or individuals in quarantine to explore their experiences, emotions, and challenges related to the disease.

b) Observations: Ethnographic observations or participant observations in healthcare settings or communities affected by COVID-19 to gain insights into behaviors, social dynamics, and cultural factors influencing the disease.

c) Focus Groups: Organizing group discussions with individuals who have experienced COVID-19 to explore common themes, shared experiences, and perceptions about various aspects of the disease, such as prevention measures, treatment, or stigma.

d) Content Analysis: Analyzing written or digital content such as social media posts, online forums, or personal diaries to extract qualitative data and understand people's attitudes, beliefs, and experiences related to COVID-19.

e) Narrative Analysis: Examining personal narratives or storytelling to capture individual experiences of COVID-19 and how it has impacted their lives.

f) Qualitative evaluation complements clinical evaluation by providing a deeper understanding of the human aspects and contextual factors surrounding the disease. It helps identify areas for improvement in public health interventions, healthcare delivery, and support systems for those affected by COVID-19.

This paper will go on to provide more detail about the specific methods used in the SC2SSP model. In this manuscript, SC2SSP is proposed. This model mentions any notable findings or contributions of the study, such as the ability of the model to identify high-risk areas for the virus or the potential for the technique to be applied to other infectious diseases. The major intention of this work is to offer a better detection rate for COVID-19 prediction at the beginning stage of diagnosis. COVID-19 has demonstrated a broad scope, affecting nearly every country and region worldwide. It has caused significant illness and mortality, overwhelmed healthcare systems, and led to various public health measures, such as lockdowns, travel restrictions, and the implementation of vaccination campaigns. The effectiveness and implementation of COVID-19 control measures vary across countries and regions. Predicting the future trajectory of control measures, such as lockdowns, mask mandates, and travel restrictions, depends on multiple factors, including vaccination coverage, public compliance, government policies, and scientific guidance. Future control measures are likely to be influenced by the progress of vaccination campaigns, ongoing surveillance, and the emergence of new variants. The proposed model begins with preprocessing the input radiographs in order to produce higher-quality source radiographs with less noise, which can be accomplished using any of the well-known image processing noise filters. The performance of SC2SSP is compared with the existing transfer learning methods. It shows an improvement in terms of accuracy as compared to other existing approaches. Simulation results illustrated in Table 6 shows that the Proposed SC2SSP model provide 4.52%, 13.82%, 9.45%, 11.45%, 12.45%, 7.67%, 15.34%, 11.2%, and 11.94% higher accuracy compared with existing methods like Sekeroglu and Ozsahin, [10], Rezaeijo *et al.*, [11], Li *et al.*, [12], Ibrahim *et al.*, [13], Cifci, [14], Irmak, [15], Rahman *et al.*, [16], Alghamdi *et al.*, [17], respectively.

Table 6. Some of the Benchmark Tables using literature support

Methods	Performance metrics Accuracy (%)
Sekeroglu and Ozsahin, [10]	0.56
Rezaeijo *et al.*, [11]	0.67
Li *et al.*, [12]	0.28
Ibrahim *et al.*, [13]	0.70
Cifci, [14]	0.70
Irmak, [15]	0.42
Rahman *et al.*, [16]	0.60
Alghamdi *et al.*, [17]	0.33
SC2SSP (proposed)	0.95

4. Challenges and Limitations

The COVID-19 pandemic has presented numerous challenges and limitations in terms of its scope and prediction. Here are some key limitations and challenges associated with understanding and predicting the spread and impact of COVID-19.

Limited Data Availability: At the early stages of the pandemic, there was a lack of comprehensive and reliable data. Testing capacities varied across regions, and underreporting or misreporting of cases and deaths was common. Limited testing, especially in asymptomatic cases, made it difficult to accurately estimate the true number of infections and assess the disease's scope.

Rapidly Evolving Nature: COVID-19 is caused by the novel coronavirus SARS-CoV-2, and at the beginning of the pandemic, there was limited knowledge about the virus, its transmission dynamics, and the effectiveness of mitigation measures. As new information emerged, public health guidelines and strategies evolved, making it challenging to predict the future course of the pandemic accurately.

Variability in Regional Responses: Different countries and regions implemented various public health measures, such as lockdowns, travel restrictions, and vaccination campaigns, leading to variations in the spread and impact of the virus. The effectiveness of these measures varied depending on factors like compliance, healthcare capacity, and socioeconomic factors, making it challenging to make precise predictions at a global scale.

Uncertain Immunity and Vaccination Effects: Understanding the long-term immunity conferred by previous infection or vaccination against COVID-19 has been an ongoing challenge. The emergence of new variants and their potential impact on vaccine effectiveness add further complexity to predicting the future trajectory of the pandemic.

Complex Interactions and Dynamics: Predicting the spread of COVID-19 involves considering complex interactions between various factors, such as population density, mobility patterns, socioeconomic disparities, healthcare infrastructure, and human behavior. Modeling these interactions accurately is challenging, and small changes in these factors can significantly impact the outcomes.

Human Behavior and Compliance: The effectiveness of containment measures relies heavily on human behavior, such as mask-wearing, social distancing, and adherence to public health guidelines. However, predicting and modeling human behavior accurately is difficult, as it is influenced by factors like cultural norms, public perception, and fatigue from prolonged restrictions.

Future Virus Variants: The emergence of new variants of SARS-CoV-2 adds another layer of uncertainty to predictions. Variants with increased transmissibility, immune evasion, or different clinical outcomes can impact the effectiveness of existing control measures and alter the trajectory of the pandemic.

However, due to the limited dataset annotations and policy limitations, the proposed method may still not take additional information into account when assessing the severity evaluation of COVID-19.

5. Conclusion

In this, a multiclass supervised learning approach was successfully implemented for predicting the severity and scope of SAR-COV2 infections. The performance of the proposed SC2SSP approach attains 12.015%, and 14.928% lower sensitivity compared with existing methods such as Resnet50 and VGGNet, respectively. The results of the study show that this approach can effectively forecast the impact of SAR-COV-2. The experimental outcomes prove that the proposed system helps clinical experts/radiologists to

support early analysis of COVID-19. Unfortunately, considering the current public health crisis, collecting the large amount of data needed to train a deep learning model is challenging. Although all openly accessible Internet datasets were used for this study, a large increase in datasets is still needed considering the number of cases reported worldwide. Nonetheless, a pure IoT-based method can create a huge count of data sets. In the future, the framework will be developed using vast X-ray images that can be further tuned with SC2SSP method.

References

1- Aswathy, A.L., Hareendran, A., SS, V.C. "COVID-19 diagnosis and severity detection from CT-images using transfer learning and back propagation neural network." *Journal of Infection and Public Health*, *14*(10), pp.1435-1445, (2021).

2- Turkoglu, M. "COVID-19 detection system using chest CT images and multiple kernels-extreme learning machine based on deep neural network." *Irbm*, *42*(4), pp.207-214, (2021).

3- Shajin, F.H., Rajesh, P., Raja, M.R. "An efficient VLSI architecture for fast motion estimation exploiting zero motion prejudgment technique and a new quadrant-based search algorithm in HEVC." *Circuits, Systems, and Signal Processing*, pp.1-24, (2022).

4- Rajesh, P., Shajin, F.H., Kumaran, G.K. "An Efficient IWOLRS Control Technique of Brushless DC Motor for Torque Ripple Minimization." *Applied Science and Engineering Progress*, *15*(3), pp.5514-5514, (2022).

5- Shajin, F.H., Rajesh, P., Nagoji Rao, V.K. "Efficient Framework for Brain Tumour Classification using Hierarchical Deep Learning Neural Network Classifier." *Computer Methods in Biomechanics and Biomedical Engineering: Imaging & Visualization*, pp.1-8, (2022).

6- Rajesh, P., Shajin, F.H., Kannayeram, G. "A novel intelligent technique for energy management in smart home using internet of things." *Applied Soft Computing*, *128*, p.109442, (2022).

7- Han, S., Roy, P.K., Hossain, M.I., Byun, K.H., Choi, C., Ha, S.D. "COVID-19 pandemic crisis and food safety: Implications and inactivation strategies." *Trends in Food Science & Technology*, *109*, pp.25-36, (2021).

8- Qiblawey, Y., Tahir, A., Chowdhury, M.E., Khandakar, A., Kiranyaz, S., Rahman, T., Ibtehaz, N., Mahmud, S., Maadeed, S.A., Musharavati, F., Ayari, M.A. "Detection and severity classification of COVID-19 in CT images using deep learning." *Diagnostics*, 11(5), p.893, (2021).

9- Fung, D.L., Liu, Q., Zammit, J., Leung, C.K.S., Hu, P. "Self-supervised deep learning model for COVID-19 lung CT image segmentation highlighting putative causal relationship among age, underlying disease and COVID-19." *Journal of Translational Medicine*, *19*, pp.1-18, (2021).

10- Sekeroglu, B., Ozsahin, I. "<? covid19?> Detection of COVID-19 from Chest X-Ray Images Using Convolutional Neural Networks." *SLAS TECHNOLOGY: Translating Life Sciences Innovation*, *25*(6), pp.553-565, (2020).

11- Rezaeijo, S.M., Ghorvei, M., Abedi-Firouzjah, R., Mojtahedi, H., Entezari Zarch, H. "Detecting COVID-19 in chest images based on deep transfer learning and machine learning algorithms." *Egyptian Journal of Radiology and Nuclear Medicine*, *52*(1), pp.1-12, (2021).

12- Li, Y., Jiang, Y., Gu, Y., Qian, P. "An Automatic Detection Method for COVID-19 in CT Images." In *Journal of Physics: Conference Series* (Vol. 2278, No. 1, p. 012044). IOP Publishing. (2022).

13- Ibrahim, M.R., Youssef, S.M., Fathalla, K.M. "Abnormality detection and intelligent severity assessment of human chest computed tomography scans using deep learning: a case study on SARS-COV-2 assessment." *Journal of Ambient Intelligence and Humanized Computing*, pp.1-24, (2021).

14- Cifci, M.A. "Deep learning model for diagnosis of corona virus disease from CT images." *Int. J. Sci. Eng. Res*, *11*(4), pp.273-278, (2020).

15- Irmak, E. "COVID-19 disease severity assessment using CNN model." *IET Image Processing*, *15*(8), pp.1814-1824, (2021).

16- Rahman, T., Akinbi, A., Chowdhury, M.E., Rashid, T.A., Şengür, A., Khandakar, A., Islam, K.R., Ismael, A.M. "COV-ECGNET: COVID-19 detection using ECG trace images with deep convolutional neural network." *Health Information Science and Systems*, *10*(1), p.1, (2022).

17- Alghamdi, H.S., Amoudi, G., Elhag, S., Saeedi, K., Nasser, J. "Deep learning approaches for detecting COVID-19 from chest X-ray images: A survey." *Ieee Access*, *9*, pp.20235-20254, (2021).

18- AKGÜN, D., KABAKUŞ, A.T., ŞENTÜRK, Z.K., ŞENTÜRK, A., KÜÇÜKKÜLAHLI, E. "A transfer learning-based deep learning approach for automated COVID-19diagnosis with audio data." *Turkish Journal of Electrical Engineering and Computer Sciences*, *29*(8), pp.2807-2823, (2021).

19- Chattopadhyay, S. "Towards grading chest X-rays of COVID-19 patients using a dynamic radial basis function network classifier." *Artificial Intelligence Evolution*, pp.81-95, (2021).

20- Tayarani, M. "Applications of artificial intelligence in battling against covid-19: A literature review." *Chaos, Solitons & Fractals*. (2020).

21- Vasal, S., Jain, S., Verma, A. "COVID-AI: an artificial intelligence system to diagnose COVID 19 disease." *J Eng Res Technol*, *9*, pp.1-6, (2020).

22- Bouchareb, Y., Khaniabadi, P.M., Al Kindi, F., Al Dhuhli, H., Shiri, I., Zaidi, H., Rahmim, A. "Artificial intelligence-driven assessment of radiological images for COVID-19." *Computers in Biology and Medicine*, *136*, p.104665, (2021).

23- Shah, P.M., Ullah, F., Shah, D., Gani, A., Maple, C., Wang, Y., Abrar, M., Islam, S.U. "Deep GRU-CNN model for COVID-19 detection from chest X-rays data." *Ieee Access*, *10*, pp.35094-35105, (2021).

24- Park, S., Kim, G., Kim, J., Kim, B., Ye, J.C. "Federated Split Vision Transformer for COVID-19 CXR Diagnosis using Task-Agnostic Training." *arXiv preprint arXiv:2111.01338*, (2021).

25- Verma, A.K., Vamsi, I., Saurabh, P., Sudha, R., Sabareesh, G.R., Rajkumar, S. "Wavelet and deep learning-based detection of SARS-nCoV from thoracic X-ray images for rapid and efficient testing." *Expert Systems with Applications*, *185*, p.115650, (2021).

26- Li, X., Geng, M., Peng, Y., Meng, L., Lu, S. "Molecular immune pathogenesis and diagnosis of COVID-19." *Journal of Pharmaceutical Analysis*, *10*(2), pp.102-108, (2020).

27- Wang, L., Lin, Z.Q., Wong, A. "Covid-net: A tailored deep convolutional neural network design for detection of covid-19 cases from chest x-ray images." *Scientific Reports*, *10*(1), pp.1-12, (2020).

28- Borakati, A., Perera, A., Johnson, J., Sood, T. "Diagnostic accuracy of X-ray versus CT in COVID-19: a propensity-matched database study." *BMJ Open*, *10*(11), p.e042946, (2020).

29- Loey, M., Manogaran, G., Khalifa, N.E.M. "A deep transfer learning model with classical data augmentation and CGAN to detect COVID-19 from chest CT radiography digital images." *Neural Computing and Applications*, pp.1-13, (2020).

30- Zheng, Z., Peng, F., Xu, B., Zhao, J., Liu, H., Peng, J., Li, Q., Jiang, C., Zhou, Y., Liu, S., Ye, C. "Risk factors of critical & mortal COVID-19 cases: A systematic literature review and meta-analysis." *Journal of Infection*, *81*(2), pp.e16-e25, (2020).

31- Wang, X., Deng, X., Fu, Q., Zhou, Q., Feng, J., Ma, H., Liu, W., Zheng, C. "A weakly-supervised framework for COVID-19 classification and lesion localization from chest CT." *IEEE Transactions on Medical Imaging*, *39*(8), pp.2615-2625, (2020).

32- Pathak, Y., Shukla, P.K., Tiwari, A., Stalin, S., Singh, S. "Deep transfer learning based classification model for COVID-19 disease." *Irbm*, *43*(2), pp.87-92, (2022).

33- Han, Z., Wei, B., Hong, Y., Li, T., Cong, J., Zhu, X., Wei, H., Zhang, W. "Accurate screening of COVID-19 using attention-based deep 3D multiple instance learning." *IEEE Transactions on Medical Imaging*, *39*(8), pp.2584-2594, (2020).

34- Ozsahin, I., Sekeroglu, B., Musa, M.S., Mustapha, M.T., Ozsahin, D.U. "Review on diagnosis of COVID-19 from chest CT images using artificial intelligence." *Computational and Mathematical Methods in Medicine*, *2020*, (2020).

35- Jin, C., Chen, W., Cao, Y., Xu, Z., Tan, Z., Zhang, X., Deng, L., Zheng, C., Zhou, J., Shi, H., Feng, J. "Development and evaluation of an artificial intelligence system for COVID-19 diagnosis." *Nature Communications*, *11*(1), p.5088, (2020).

36- Ahuja, S., Panigrahi, B.K., Dey, N., Rajinikanth, V., Gandhi, T.K. "Deep transfer learning-based automated detection of COVID-19 from lung CT scan slices." *Applied Intelligence*, *51*, pp.571-585, (2021).

37- Xiao, L.S., Li, P., Sun, F., Zhang, Y., Xu, C., Zhu, H., Cai, F.Q., He, Y.L., Zhang, W.F., Ma, S.C., Hu, C. "Development and validation of a deep learning-based model using computed tomography imaging for predicting disease severity of coronavirus disease 2019." *Frontiers in Bioengineering and Biotechnology*, *8*, p.898, (2020).

38- Pu, J., Leader, J.K., Bandos, A., Ke, S., Wang, J., Shi, J., Du, P., Guo, Y., Wenzel, S.E., Fuhrman, C.R., Wilson, D.O. "Automated quantification of COVID-19 severity and progression using chest CT images." *European Radiology*, *31*, pp.436-446, (2021).

39- Shen, C., Yu, N., Cai, S., Zhou, J., Sheng, J., Liu, K., Zhou, H., Guo, Y., Niu, G. "Quantitative computed tomography analysis for stratifying the severity of Coronavirus Disease 2019." *Journal of Pharmaceutical Analysis*, *10*(2), pp.123-129, (2020).

40- Shan, F., Gao, Y., Wang, J., Shi, W., Shi, N., Han, M., Xue, Z., Shen, D., Shi, Y. "Abnormal lung quantification in chest CT images of COVID-19 patients with deep learning and its application to severity prediction." *Medical Physics*, *48*(4), pp.1633-1645, (2021).